crystals

MDPI

Article

New Co-Crystals/Salts of Gallic Acid and Substituted Pyridines: An Effect of Ortho-Substituents on the Formation of an Acid–Pyridine Heterosynthon

Gleb L. Denisov [1,2] and Yulia V. Nelyubina [1,2,*]

[1] A.N. Nesmeyanov Institute of Organoelement Compounds, Russian Academy of Sciences, Vavilova Str., 28, 119991 Moscow, Russia; denisov0gleb@gmail.com
[2] Bauman Moscow State Technical University, Baumanskaya Str., 5, 105005 Moscow, Russia
* Correspondence: unelya@ineos.ac.ru

Abstract: Co-crystallization of gallic acid with pyridines and their polyaromatic analogue, quinoline, ortho-substituted by various proton-donating groups able to form hydrogen bonds, produced the only reported co-crystal of gallic acid with an *ortho*-substituted pyridine, 2-hydroxypyridine, as its preferred pyridone-2 tautomer, and four new crystalline products of gallic acid. These co-crystals, or gallate salts depending on the choice of the pyridine-containing compound, as predicted by the pKa rule, were identified by X-ray diffraction to feature the popular acid–pyridine heterosynthon found in most of the two-component systems of gallic acid that lack *ortho*-substituents in the pyridine-containing compound. This single-point heterosynthon is, however, modified by one or two proton-donating *ortho*-substituents, which sometimes may transform into the proton acceptors in an adopted tautomer or zwitterion, to produce its two- or other multi-point variants, including a very rare four-point heterosynthon. The hydrogen bonds they form with the gallic acid species in the appropriate co-crystals/salts strongly favors the formation of the acid–pyridine heterosynthon over the acid–acid homosynthon. In the competitive conditions of multi-component systems, such a modification might be used to reduce supramolecular-synthon-based polymorphism to produce new pharmaceuticals and other crystalline materials with designed properties.

Keywords: co-crystals; crystal engineering; heterosynthon; hydrogen bond; gallic acid; multi-point heterosynthon; pyridine; supramolecular synthon; X-ray diffraction

Citation: Denisov, G.L.; Nelyubina, Y.V. New Co-Crystals/Salts of Gallic Acid and Substituted Pyridines: An Effect of Ortho-Substituents on the Formation of an Acid–Pyridine Heterosynthon. *Crystals* **2022**, *12*, 497. https://doi.org/10.3390/cryst12040497

Academic Editors: Sławomir Grabowski and Duane Choquesillo-Lazarte

Received: 11 March 2022
Accepted: 1 April 2022
Published: 3 April 2022

1. Introduction

Crystal engineering, the design of molecular solids [1], exploits supramolecular structures self-assembled [2] by intermolecular interactions [3–7], such as hydrogen bonds [8–11], to produce crystalline materials of various topologies and applications [12–18]. Among others [19], carboxylic acids that are both donors and acceptors of hydrogen bonds [19] form several stable supramolecular associates (or synthons [7]) with complementary functional groups, including pyridyl- [20], amino- [21] and hydroxyl [22] groups, providing control over the crystal packing, and thereby the properties, of such materials [23].

Trihydroxybenzoic (gallic) acid, a component of metal–organic framework compounds (MOFs) found in historical iron–gall inks [24], is a naturally occurring [25,26] antioxidant, antiviral, and antitumor agent [27–35]. It is also a popular co-former in pharmaceutical co-crystals and salts [32,36] used to improve the solubility [37–39] and the bioactivity [38,40,41] of drug compounds through the formation of stable hydrogen-bonded associates [42,43]. Most of these two-component systems [44,45], as well as those of 3,5-dihydroxybenzoic acid [22,46], a close analog of gallic acid [22], and of other functionalized benzoic acids [47–49] are formed by the well-known supramolecular [7] acid–pyridine heterosynthon, either neutral or ionic [47,50,51] (Scheme 1, left). The latter is further stabilized by a pyridine compound containing proton-donating groups in the *ortho*-positions to

produce a two- or multi-point heterosynthon (Scheme 1, right), depending on the number of hydrogen bonds between the two species [10,22,52]. As is the motivation behind the synthon concept [7], the knowledge of possible variations of this heterosynthon often enabled predicting the crystal packing even in the presence of other functional groups able to form competitive hydrogen bonds [10,22,50,52].

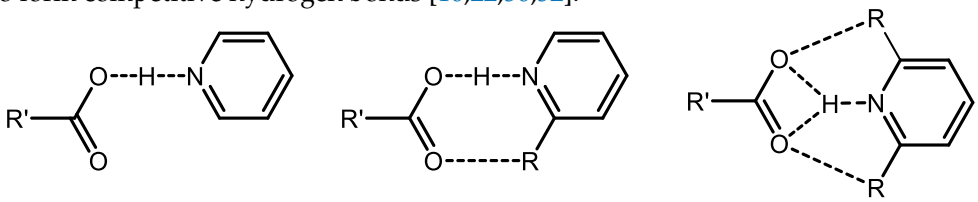

Scheme 1. Single- (**left**), two- (**center**), and four- (**right**) point heterosynthons formed by gallic acid and pyridine and its derivatives with proton-donating groups R in the *ortho*-position.

Co-crystallization of a carboxylic acid with a pyridine compound may produce either a co-crystal [53] built by neutral components or a salt featuring the proton transfer from acid to base [54,55], both useful in the pharmaceutical industry [56–58]. Although such two-component systems are widely studied in supramolecular chemistry [59], only a few reports exist on those formed by gallic acid, including co-crystals [41,60–63] and salts [60,63–66], and none of them contain an *ortho*-substituted pyridine except for 2-hydroxypyridine [63]. In an appropriate co-crystal, the latter exists as the preferred tautomer [67,68], pyridone-2 (Scheme S1 of supplemantary), that forms with gallic acid the typical two-point heterosynthon (Scheme 1, center) [63].

Following this recent study [63], we attempted to co-crystallize gallic acid (Scheme 2) with 2-hydroxypyridine (**2-OH-Py**) and other pyridines *ortho*-functionalized by proton-donating groups, such as commercially available 2,6-diaminopyridine (**2,6-NH2-Py**) and 2,6-dimethylhydroxypyridine (**2,6-CH2OH-Py**), as well as quinoline-2-carboxylic acid (**2-COOH-quinoline**), with an extended polyaromatic system to induce stacking interactions between the two components, another type of intermolecular interactions for creating tunable crystalline materials, including organic co-crystals and polymorphs [69–71]. Their co-crystallization with gallic acid in methanol or, alternatively, acetonitrile, produced the previously reported co-crystal of pyridone-2 [63], which was obtained under similar crystallization conditions in methanol or by liquid-assisted grinding, and four new crystalline products of gallic acid, including a new solvatomorph of this co-crystal. Different functional groups able to form competitive hydrogen bonds in the *ortho*-position(s) of the pyridine ring in these heterocyclic compounds and a methylene bridge in **2,6-CH2OH-Py** for additional flexibility enable modulation of the crystal environment of gallic acid to probe its effect on the formation of the above heterosynthon (Scheme 1) by X-ray diffraction analysis of the co-crystals or salts obtained as a function of the *ortho*-substituted pyridine.

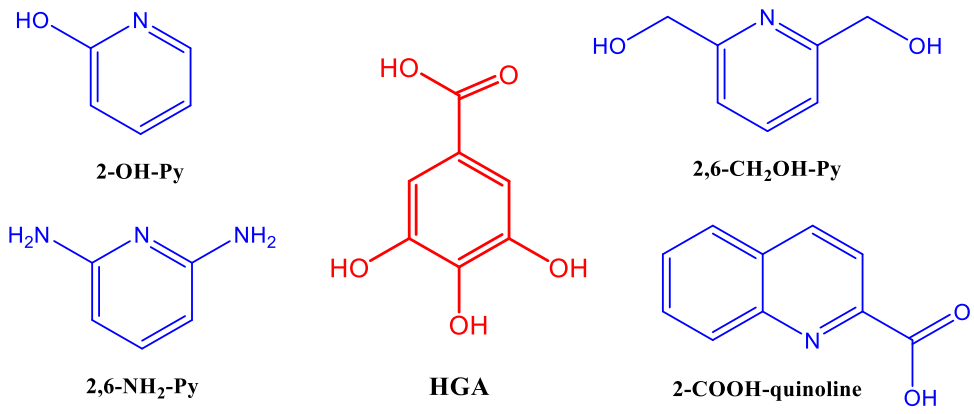

Scheme 2. Organic components in this study.

2. Materials and Methods

Synthesis. All synthetic procedures were carried out in air. Gallic acid (**GA**), 2-hydroxypyridine (**2-OH-Py**), 2,6-diaminopyridine (**2,6-NH_2-Py**), 2,6-dimethylhydroxypyridine (**2,6-CH_2OH-Py**), quinoline-2-carboxylic acid (**2-COOH-quinoline**), and solvents were purchased from commercial sources and used without any further purification. Carbon, nitrogen, and hydrogen contents were measured with a Carlo Erba microanalyzer, model 1106 (Carlo Erba Instruments, Egelsbach, Germany).

[HGA][2-O-PyH] (**1**) **+ [HGA][2-O-PyH][CH_3CN]$_2$** (**2**): In a 1.6 mL glass vial, gallic acid (0.0034 g; 0.02 mmol) and 2-hydroxypyridine (0.0021 g; 0.02 mmol) were dissolved in acetonitrile (0.6 mL). After six days of slow evaporation at room temperature in the tightly closed vial, colorless plate-like crystals of **1** were collected from the bottom of the vial. Yield: 30 mg (55%). Anal. Calc. for $C_{12}H_{11}NO_6$ (%): C, 54.34; H, 4.18; N, 5.28. Found (%): C, 54.37; H, 4.33; N, 5.58. Three weeks later, colorless needles of **2** were collected from the walls of the vial. Yield: 9 mg (16%). Anal. Calc. for $C_{16}H_{17}N_3O_6$ (%): C, 55.33; H, 4.93; N, 12.10. Found (%): C, 55.35; H, 4.52; N, 11.85.

[HGA][2-COO-quinolineH] (**3**): In a 1.6 mL glass vial, gallic acid (0.0017 g; 0.01 mmol) and quinoline-2-carboxylic acid (0.0018 g; 0.01 mmol) were dissolved in methanol (0.6 mL). After ten days of slow evaporation at room temperature in a tightly closed vial, yellow needle-like crystals of **3** were collected from the walls of the vial. Yield: 0.0033 mg (94%). Anal. Calc. for $C_{17}H_{13}NO_7$ (%): C, 59.48; H, 3.82; N, 4.08. Found (%): C, 59.67; H, 4.02; N, 4.38.

[GA][2,6-NH_2-PyH][CH_3CN]$_{0.416}$ (**4**): In a 1.6 mL glass vial, 2,6-diaminopyridine (0.0022 g; 0.02 mmol) was dissolved in hot acetonitrile (0.6 mL). The pale-green solution was decanted from undissolved dark-green pyridine and added to gallic acid (0.0034 g; 0.02 mmol). After six days of slow evaporation at room temperature in the tightly closed vial, large colorless prismatic crystals of **4** were collected. Yield: X 0.0014 (25%). Anal. Calc. for $C_{12.83}H_{14.25}N_{3.42}O_5$ (%): C, 53.42; H, 4.38; N, 14.38. Found (%): C, 51.52; H, 4.66; N, 15.55.

[GA][2,6-CH_2OH-PyH] (**5**): In a 1.6 mL glass vial, gallic acid (0.0034 g; 0.02 mmol) and 2,6-dimethylhydroxypyridine (0.0029 g; 0.02 mmol) were dissolved in acetonitrile (0.6 mL). After three weeks of slow evaporation at room temperature in a tightly closed vial, colorless plate-like crystals were collected from the bottom of the vial. Yield: 0.0020 mg (32%). Anal. Calc. for $C_{14}H_{15}NO_7$ (%): C, 54.37; H, 4.89; N, 4.53. Found (%): C, 56.37; H, 5.71; N, 6.83.

X-ray crystallography. Single crystals of **1**–**5** suitable for X-ray diffraction analysis were obtained in the above crystallization conditions. X-ray diffraction data for **1**, **2**, **4**, and **5** were collected at 120 K with a Bruker APEXII DUO CCD diffractometer (Bruker AXS, Madison, USA); those for **3** were collected at 100 K with a Bruker D8 Quest CMOS diffractometer, both using the graphite monochromated Mo-Kα radiation (λ = 0.71073 Å, ω-scans). Using Olex2 [72], the structures were solved with the ShelXT [73] structure solution program using Intrinsic Phasing and refined with the XL refinement package [74] using Least Squares minimization against F^2 in anisotropic approximation for non-hydrogen atoms. Hydrogen atoms of NH and OH groups were found in the difference Fourier synthesis while the positions of other hydrogen atoms were calculated, and they all were refined in the isotropic approximation within the riding model. The 'head-to-tail' disorder of the solvate acetonitrile molecule in **4** was modeled using DFIX, EADP, and SADI instructions. Crystal data and structure refinement parameters are given in Table 1. CCDC 2151555–2151559 contain the supplementary crystallographic data for of **1**–**5**.

Table 1. Crystal data and structure refinement parameters for **1**–**5**.

Parameter	1	2	3	4	5
Formula unit	$C_{12}H_{11}NO_6$	$C_{16}H_{17}N_3O_6$	$C_{17}H_{13}NO_7$	$C_{12.83}H_{14.25}N_{3.42}O_5$	$C_{14}H_{15}NO_7$
Formula weight	265.22	347.32	343.28	296.36	309.27
Temperature, K	120	120	100	120	120
Crystal system	Monoclinic	Triclinic	Monoclinic	Triclinic	Monoclinic
Space group	$P2_1/c$	P-1	$P2_1/c$	P-1	$P2_1/n$
Z	4	2	4	4	4
a, Å	13.003(4)	7.4243(9)	8.6047(3)	8.7264(17)	7.2058(12)
b, Å	15.819(5)	7.9649(10)	24.5784(7)	11.645(2)	24.941(4)
c, Å	13.037(5)	14.5075(18)	9.6157(4)	14.032(3)	7.7817(13)
α, °	90	103.247(3)	90	84.710(4)	90
β, °	155.854(6)	102.030(3)	135.550(2)	76.573(4)	111.937(3)
γ, °	90	90.662(3)	90	74.909(4)	90
V, Å^3	1096.8(6)	815.13(18)	1424.11(9)	1338.3(4)	1297.3(4)
D_{calc} (g cm^{-3})	1.606	1.415	1.601	1.471	1.583
Linear absorption, μ (cm^{-1})	1.31	1.10	1.27	1.15	1.29
F(000)	552	364	712	621	648
$2\Theta_{max}$, °	52	54	54	52	54
Reflections measured	10,262	8783	11,930	13,215	12,477
Independent reflections	2153	3551	3071	5262	2750
Observed reflections [I > 2σ(I)]	1187	2546	2328	2597	1877
Parameters	174	228	226	398	199
R1	0.0565	0.0488	0.0463	0.0683	0.0465
wR2	0.1490	0.1207	0.1127	0.2101	0.1069
GOF	0.970	1.048	1.022	1.038	0.905
$\Delta\rho_{max}/\Delta\rho_{min}$ (e Å^{-3})	0.263/−0.411	0.296/−0.343	0.324/−0.288	0.627/−0.531	0.235/−0.291

3. Results and Discussion

The appropriate *ortho*-substituted pyridines, 2-hydroxypyridine (**2-OH-Py**), 2,6-diaminopyridine (**2,6-NH_2-Py**), and 2,6-dimethylhydroxypyridine (**2,6-CH_2OH-Py**), and their polyaromatic analogue, quinoline-2-carboxylic acid (**2-COOH-quinoline**), were each dissolved together with gallic acid in a 1:1 ratio in a suitable solvent, acetonitrile, or methanol commonly used for evaporative crystallization [75], among others, to produce the reported co-crystal of gallic acid and pyridone-2 [63]. The resulting solutions were kept in tightly closed glass vials at room temperature for up to four weeks, and the vials were visually inspected every 2–3 days to follow the formation of crystalline products. Their subsequent X-ray diffraction analysis identified, in addition to the previously reported co-crystal **1** of pyridone-2 [63], four new two-component systems based on gallic acid, the co-crystals **2** (**[HGA][2-O-PyH][CH_3CN]$_2$**) and **3** (**[HGA][2-COO-quinolineH]**) and the salts **4** (**[GA][2,6-NH_2-PyH][CH_3CN]$_{0.416}$**) and **5** (**[GA][2,6-CH_2OH-PyH]**).

The first two were collected from the same vial at different time periods of the co-crystallization of gallic acid with **2-OH-Py**, which resulted in colorless plate-like crystals of **1** on the bottom of the vial and, after some time in the mother liquor, in colorless needle-like crystals of **2** on its walls. Both co-crystals, the previously reported **1** [63] and its new solvatomorph **2** with two molecules of lattice acetonitrile, contain **2-OH-Py** as pyridone-2 and gallic acid in a 1:1 ratio (Figure 1, top). The two species are connected by O-H ... O and N-H ... O hydrogen bonds (O ... O 2.563(8) and 2.6062(19) Å, OHO 162.39(15) and 168.73(9)°; N ... O 2.941(8) and 2.798(2) Å, NHO 154.7(2) and 175.82(9)°) to produce the expected two-point acid–pyridine heterosynthon [47] (Scheme 1, center). An additional O-H ... O hydrogen bond between one hydroxyl group of gallic acid and the oxygen atom of pyridone-2 (O ... O 2.640(3) and 2.6772(18) Å, OHO 163.2(4) and 168.58(9)° in **1** and **2**, respectively) assembles them into a heterotetramer (Figure 1, bottom). In **2**, the latter is decorated by four solvate acetonitrile molecules (Figure 1, bottom right) via O-H ... N hydrogen bonds with the other two hydroxyl groups of gallic acid (O ... N 2.810(2) and 2.876(2) Å, NHO 146(10) and 170(9)°). In the previously reported co-crystal **1** [63], such heterotetramers form a zigzag-like 3D-framework (Figure 1, bottom

left) by O-H . . . O hydrogen bonds between the acid molecules (O . . . O 2.763(5)–2.89(1) Å, OHO 130.20(16)–143.06(17)°). In **2**, however, they are hold together by parallel-displaced stacking interactions between the aromatic fragments of pyridone-2 and gallic acid with the inter-centroid and shift distances of 3.6319(9) and 1.518(2) Å, respectively, and the angle of 4.30(6)°.

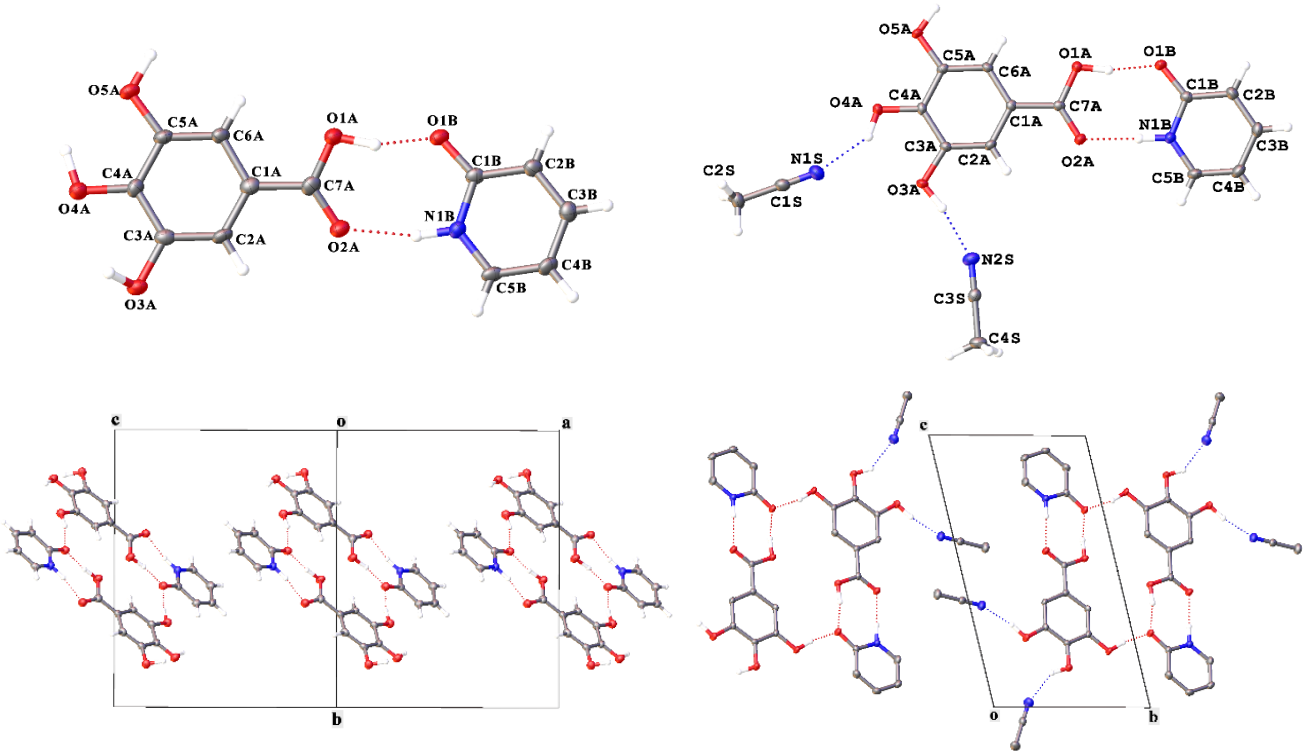

Figure 1. General views of **1** (**top left**) and **2** (**top right**) and fragments of the crystal packing in **1** (**bottom left**) and **2** (**bottom right**), illustrating the formation of hydrogen-bonded heterotetramers. Hereinafter, non-hydrogen atoms are shown as thermal ellipsoids (p = 50%) and dashed lines stand for hydrogen bonds.

The third co-crystal, **3**, was obtained when an equimolar mixture of gallic acid and **2-COOH-quinoline** was stored under similar conditions in methanol, as the use of acetonitrile led to the formation of an amorphous powder. The resulting yellow needle-like crystals of the composition **[HGA][2-COO-quinolineH]** with the molecule of gallic acid and the quinoline zwitterion (Figure 2, top), as identified by X-ray diffraction, feature the same two-point heterosynthon formed by N-H . . . O and O-H . . . O hydrogen bonds (O . . . O 2.6601(18) Å, OHO 172.95(17)°; N . . . O 2.739(2) Å, NHO 160.73(17)°). The hydroxyl groups of gallic acid bind it to the four neighboring species of **2-COO-quinolineH** and gallic acid by using their carboxylate and hydroxyl groups (O . . . O 2.604(4)–2.9914(19) Å, OHO 144.01(15)–158.29(10)°) to produce hydrogen-bonded double layers that run parallel to the diagonal of the crystallographic plane *ac* (Figure 2, bottom); those are additionally stabilized by parallel-displaced stacking interactions between the molecules of gallic acid and the quinoline zwitterions with inter-centroid and shift distances of 3.8027(10) and 1.803(2) Å and an angle of 1.63(4)°. The layers are held together by similar stacking interactions with the inter-centroid and shift distances of 3.3893(8) and 0.880(2) Å and an angle of 1.63(4)°.

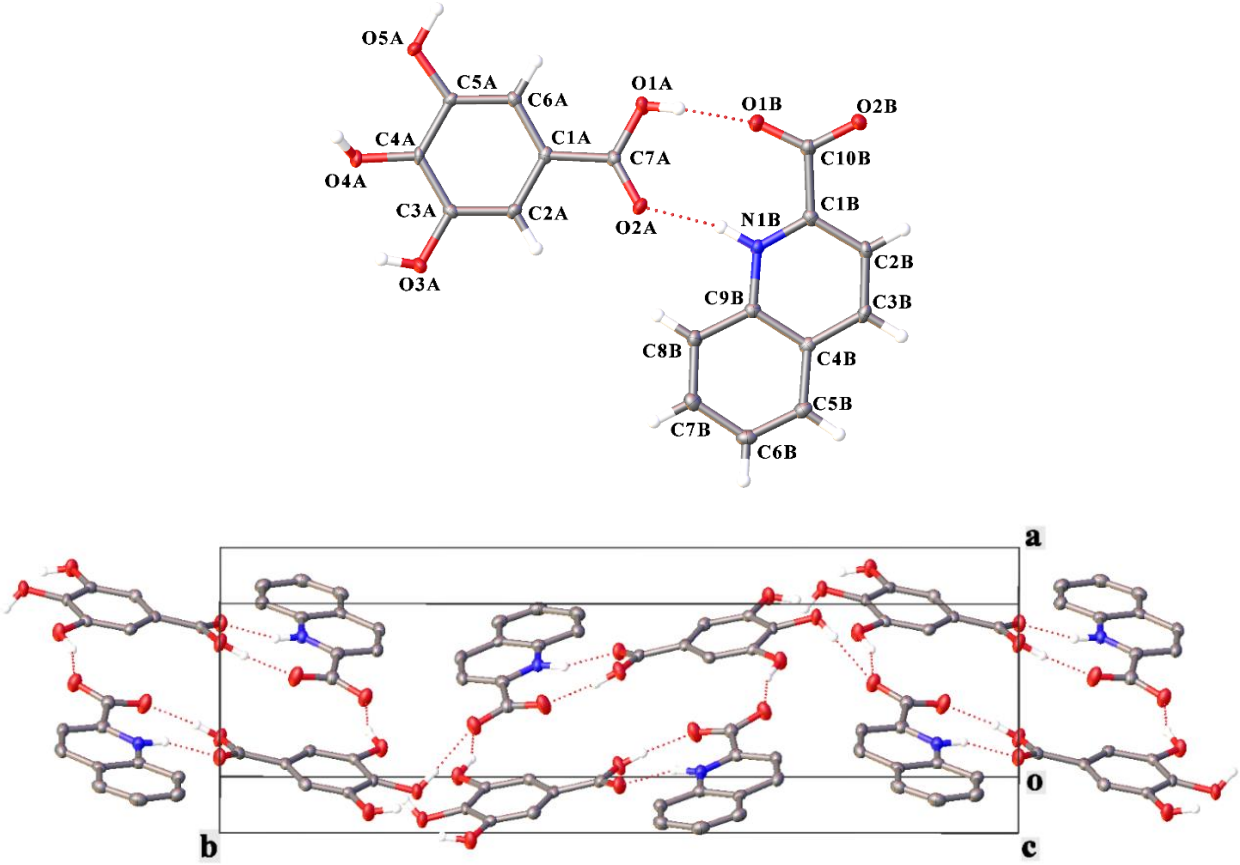

Figure 2. General view of **3** (**top**) and a fragment of its crystal packing (**bottom**), illustrating the formation of hydrogen-bonded double layers.

In contrast, the co-crystallization of gallic acid with the pyridines **2,6-NH_2-Py** and **2,6-CH_2OH-Py** *ortho*-functionalized by two proton-donating groups resulted, after one or three weeks in acetonitrile, in the salts **4** (**[GA][2,6-NH_2-PyH][CH_3CN]$_{0.416}$**) and **5** (**[GA][2,6-CH_2OH-PyH]**). Despite spending less time in a mother liquor, the former was obtained as a crystallosolvate with two symmetry-independent formula units of the salt and a disordered molecule of acetonitrile partially occupying an appropriate position in the unit cell. In both cases (Figure 3, top), the gallate anions and the pyridinium cations are held together by N-H . . . O and O-H . . . O hydrogen bonds (N . . . O 2.766(4)–3.034(2) Å, NHO 124.28(11)–177.6(2)°; O . . . O 2.642(2)–2.737(2) Å, OHO 152.41(8)–166.83(10)°) to produce a rare [76,77] four-point (Figure 3, top left) or a typical [48,50] two-point (Figure S1 of Supplementary Materials) acid–pyridine heterosynthon in **4** and a less common [78,79] three-point heterosynthon in **5**. In the latter salt, an unfavorable geometry of the hydrogen bond N-H . . . O (Figure 3, top left) is, apparently, induced by the methylene bridges in the *ortho*-substituents of **2,6-CH_2OH-PyH** that make the aromatic fragments of the counterions occupy almost parallel planes inclined at an angle of 1.23(9)°. In all the above crystalline products, this angle does not exceed 4.5°.

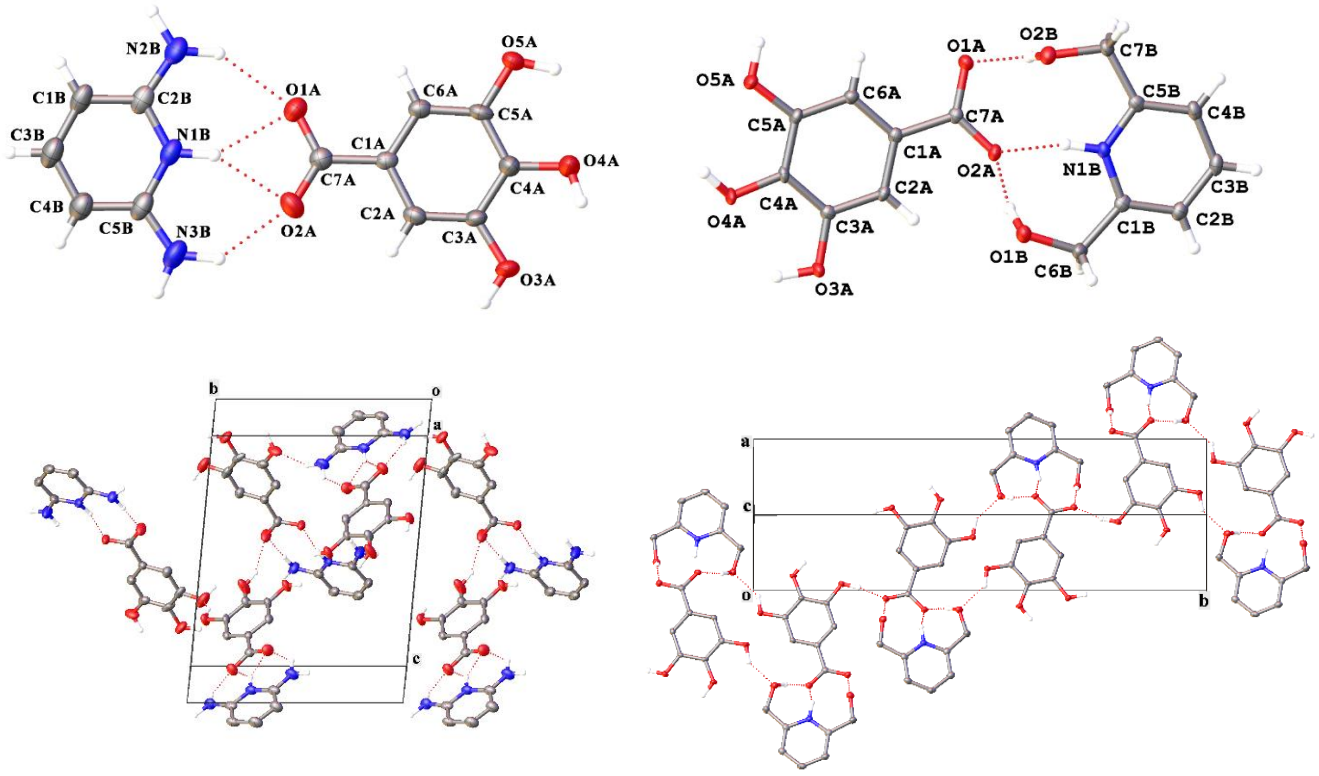

Figure 3. General views of **4** (**top left**) and **5** (**top right**) with second symmetry-independent species of **4** and a disordered molecule of acetonitrile omitted for clarity and fragments of the crystal packing in **4** (**bottom left**) and **5** (**bottom right**) illustrating the formation of hydrogen-bonded interpenetrating network and double layers, respectively. For the general view of the second symmetry-independent formula unit of **4**, see Figure S1 of Supplementary Materials.

In the crystal of the salt **5**, such an arrangement of the two species in the acid–pyridine heterosynthon results in the formation of double layers (Figure 3, bottom right) via hydrogen bonds O-H . . . O between the two hydroxyl groups and the carboxyl group of the gallate anions (O . . . O 2.6637(18)–2.667(2) Å, OHO 147.58(11)–159.48(12)°), and between the third hydroxyl group of the gallate anion and one of the hydroxyl groups of the cation (O . . . O 2.7577(18) Å, OHO 140.09(9)°). These hydrogen-bonded double layers are additionally stabilized by parallel-displaced stacking interactions between the gallate anions and cations (Figure 3, bottom right), with inter-centroid and shift distances of 3.4999(15) and 1.023(4) Å and an angle of 1.23(9)°. The layers are held together by similar stacking interactions, with inter-centroid and shift distances of 3.7510(14) and 1.819(4) Å and an angle of 1.23(9)°.

In the crystal of the salt **4**, the four-point heterosynthon (Figure 3, top left) forms heterotetramers similar to those found in the co-crystals **1** and **2** (Scheme 1, center) via hydrogen bonds N-H . . . O (N . . . O 3.052(5) Å, NHO 151.6(2)°) between the amino group of the pyridinium cation and the hydroxyl group of the gallate anion. These heterotetramers are packed into infinite columns that run perpendicular to the diagonal of the crystallographic plane *bc* (Figure S2 of Supplementary Materials) by parallel-displaced stacking interactions featuring inter-centroid and shift distances of 3.598(2) Å and 1.054(6) Å and an angle of 4.69(13)°. The two-point heterosynthons do not interact with each other (Figure S2 of Supplementary Materials). However, as the two symmetry-independent formula units of the salt **4** are perpendicular (the angle between their mean planes is 89.94(5)°), the two types of heterosynthons are connected by multiple O-H . . . O (O . . . O 2.091(5)–2.583(3) Å, OHO 153.2(2)–164.21(17)°) and N-H . . . O (N . . . O 2.984(5)–3.023(5) Å, NHO 139.0(3)–154.3(3)°) hydrogen bonds to produce an interpenetrating hydrogen-bonding network (Figure 3,

bottom left). In its voids reside solvate acetonitrile molecules that are disordered in a 'head-to-tail' mode, thus forming hydrogen bonds either with the pyridinium cation (N ... N 2.830(12) Å, NHN 156.1(5)°) or the gallate anion (O ... N 3.156(19) Å, OHN 167.8(4)°).

In all the above crystalline products of gallic acid, the latter forms the well-known [50] acid–pyridine heterosynthon (Scheme 1, left) modified by proton-donating functional groups close to the heterosynthon-producing nitrogen atom of the pyridine fragment to produce its two-, three-, and four-point variants (Scheme 1, right). The first two are often found [47,78,79] between a carboxylic acid and a pyridine with one or two *ortho*-substituents. In rare cases [76,77], the four-point heterosynthon is observed when both the components are located in the same plane as close as possible to the axial symmetry, which is adopted by one symmetry-independent formula unit of the salt **4**. In this salt, the competition between the two identical proton-donating groups in the *ortho*-positions of the pyridine fragment that cannot simultaneously fulfil all of their potential by one-to-one hydrogen bonding [80] to the carboxylate group allows for the formation of an asymmetric two-point heterosynthon by the horizontal shift of the gallate anion in the plane occupied by the two components.

The resulting differences in the crystalline environment of the molecule of gallic acid or the gallate anion can be nicely visualized by Hirshfeld surfaces [81] and quantified by their two-dimensional (2D) fingerprint plots [82]. In the co-crystals **1**–**3** with the same two-point heterosynthon, the bright red spots on the Hirshfeld surfaces of the molecule of gallic acid (Figure 4, left) correspond to O ... H contacts with the neighboring acid molecules and those with the pyridine-2 molecules and the zwitterions of quinoline-2-carboxylic acid. They appear on the appropriate 2D fingerprint plots (Figure 4, right) as the most populated forceps-like areas, accounting for 44.7, 39.8, and 44.6% of the Hirshfeld surface in **1**, **2**, and **3**, respectively (Table 2). The other types of major contributors are H ... H (25.2, 24.5, and 24.3%), C ... H (15.9, 11.7, and 8.5%), and C ... O (7.6, 6.4, and 7.3%) contacts. In the co-crystal **3**, they are supplemented by C ... C contacts (12.4% vs. 2.1 and 4.9% in **1** and **2**), which appear as flat white areas on the Hirshfeld surface of the molecule of gallic acid (Figure 4, left) approached by an extended aromatic system of the zwitterions of quinoline-2-carboxylic acid. A significantly larger contribution of N ... H contacts in the new solvatomorph **2** of the reported co-crystal **1** (8.7% vs. 0.6 and 0.7% in **1** and **3**, respectively) arises from the presence of lattice acetonitrile molecules. The contribution of other types of interactions formed by the molecule of gallic acid in the three co-crystals (Table 2) is below 3.1%.

Table 2. Contributions (%) of various interactions into the Hirshfeld surface of the gallic acid molecule in the co-crystals **1**, **2**, and **3**.

Contacts	1	2	3	Average
O ... H	44.7	39.8	44.6	43.0
N ... H	0.6	8.7	0.7	3.3
C ... H	15.9	11.7	8.5	12.0
H ... H	25.2	24.5	24.3	24.7
C ... C	2.1	4.9	12.4	6.5
O ... O	3.1	0.6	0.6	1.4
C ... N	0.4	2.6	1.6	1.5
C ... O	7.6	6.4	7.3	7.1
N ... O	0.6	0.7	0.0	0.4

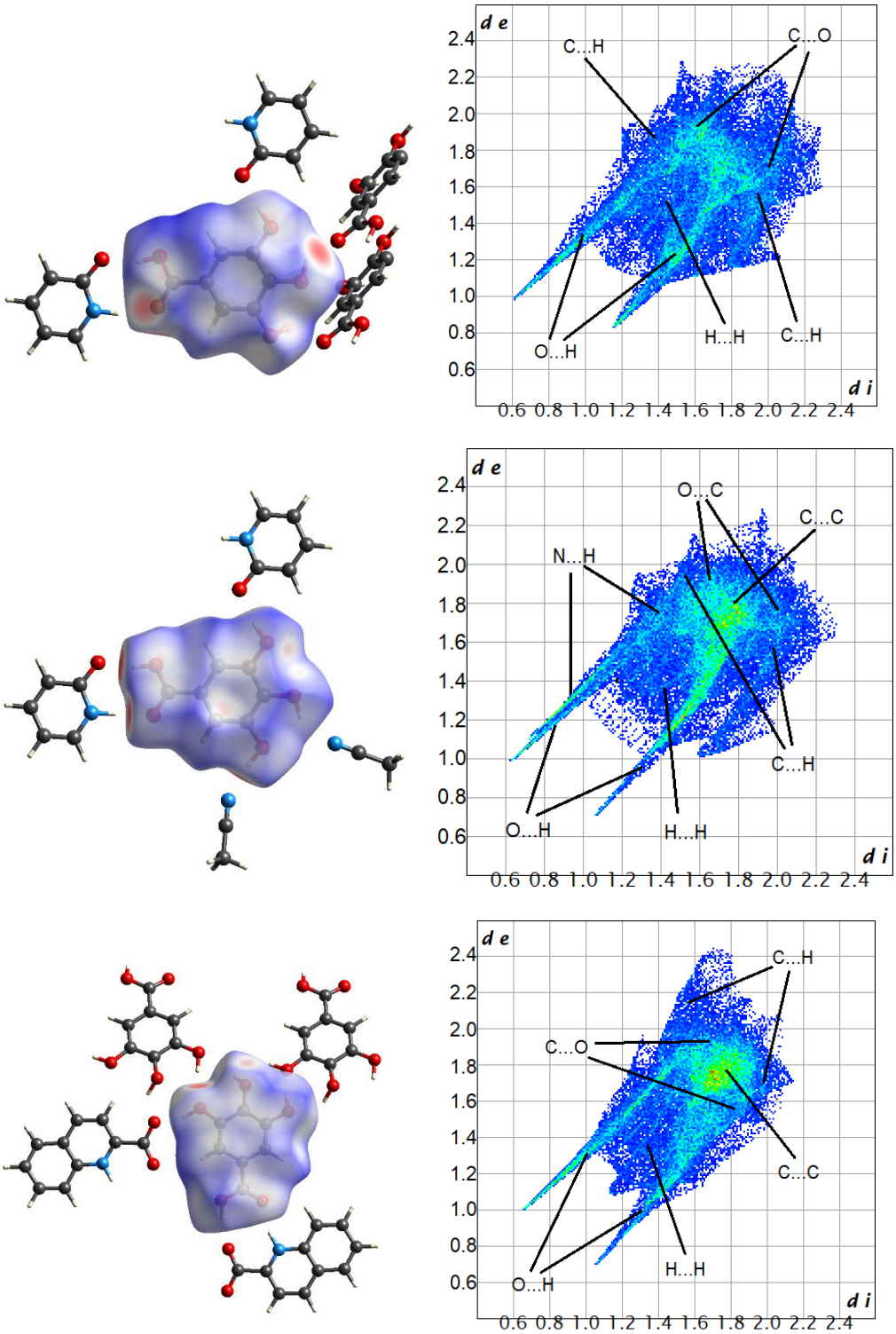

Figure 4. Hirshfeld surfaces (**left**) of the gallic acid molecule in the co-crystals **1** (**top**), **2** (**center**), and **3** (**bottom**) and their 2D fingerprint plots (**right**) as generated by Crystal Explorer [83]. Hereinafter, on the Hirshfeld surfaces (**left**), the red, white, and blue color recognizes the interatomic contacts as shorter than, equal to, or longer than the van der Waals interatomic distances, respectively. On fingerprint plots (**right**), higher and lower concentrations of points corresponding to (d_i, d_e) pairs are shown by green and blue areas, respectively; interactions with a total contribution of less than 3% are not designated.

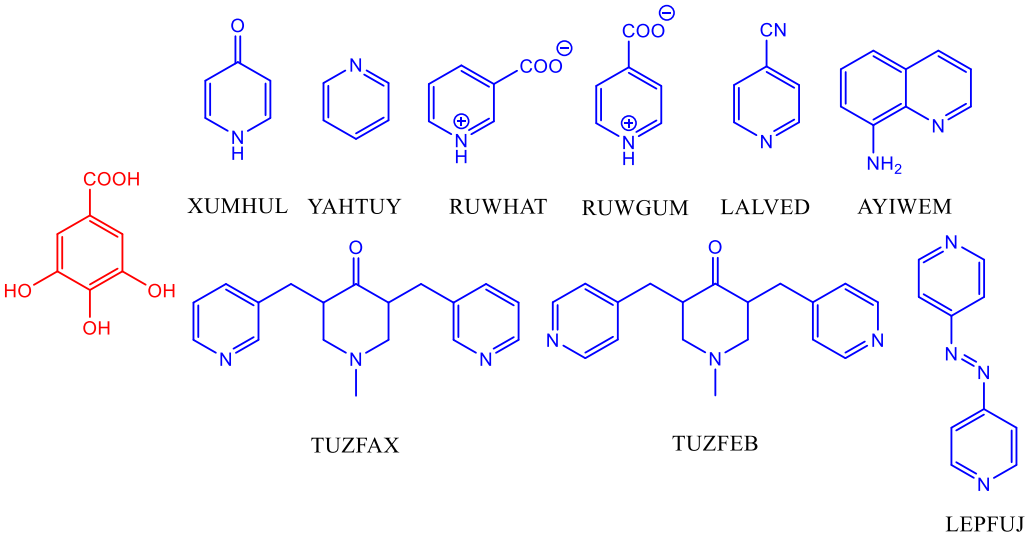

Scheme 3. Co-crystals of gallic acid and pyridine-containing compounds and their RefCodes [41,60,62,85]; XUMHUL, RUWHAT, RUWGUM, TUZFAX, and LEFPUJ also contain solvate molecules of water and methanol, respectively.

The obtained co-crystals **1**–**3** featuring the two-point acid–pyridine heterosynthon (Scheme 1, center) are in a stark contrast to other reported (ordered) co-crystals of gallic acid and pyridine-containing compounds available in the Cambridge Structural Database (CCDC Version 2021.2.0) (Cambridge, UK), which all lack the *ortho*-substituents in the pyridine fragment (Scheme 3) [41,60,62] and thereby produce the single-point acid–pyridine heterosynthon (Scheme 1, left) or other, competing synthons. An acid–acid homosynthon, which is often formed by carboxylic acids in the presence of pyridines [84], assembles the molecules of gallic acid in its co-crystals with 4-hydroxypyridine (RefCode XUMHUL [63]) as its 4-pyridone tautomer, nicotinic and isonicotinic acids (RUWHAT and RUWGUM [61]), and quinoline-8-amine (AYIWEM) (Figures S3–S5 of Supplementary Materials). As a result, the crystal environment of gallic acid (Figure S6 of Supplementary Materials) is significantly different from those in **1**–**3**, as hinted, e.g., by a very small contribution of the N ... H contacts into its Hirshfeld surface (Table S1 of Supplementary Materials). In RUWHAT and RUWGUM [61], the occurrence of a single-point acid–pyridine heterosynthon between the zwitterions of nicotinic and isonicotinic acids (Figure S4 of Supplementary Materials) could be related to its higher strength (N ... O 2.575(5) and 2.6232(18) Å, NHO 172.6(3) and 174.04(10)°) as compared to an average gallic acid–pyridine heterosynthon (Tables S2 and S3 of Supplementary Materials).

With all the other pyridine-containing compounds (Scheme 3), gallic acid forms the expected single-point acid–pyridine heterosynthon that has various packing motifs in the co-crystals depending on structural features of the heterocyclic component and/or the presence of lattice solvents. Thus, meta- and para-substitution of the two pyridine fragments in the co-crystals TUZFAX [60] and TUZFEB [60] (the former, as a hydrate) leads to the formation of heterotetramers or zig-zag chains by joining such heterosynthons via hydrogen bonds with one of the hydroxyl groups of gallic acid (Figure S7 of Supplementary Materials). A hydrogen bond of the other with the third nitrogen atom in the pyridine-containing compound assembles them into layers, with the phenyl ring of gallic acid being either coplanar to one of the pyridine fragments (and, therefore, involved in parallel-displaced stacking interactions) or almost perpendicular to both. Such an arrangement of the two components results in different contributions of intermolecular interactions into the Hirshfeld surface of the molecule of gallic acid, such as a dramatic decrease in the contribution of the C ... C contacts from 9.7% in TUZFAX to 0.8% in TUZFEB (Table S1). In the co-crystal with 1,2-bis(pyridin-4-yl)diazene (LEFPUJ [85]), its two symmetry-independent species are hydrogen-bonded either to two molecules of gallic acid in the same way as in TUZFAX and

TUZFEB or to only one such molecule and lattice methanol, thereby producing layers with alternating chains made of the two components (Figure S8 of Supplementary Materials). In these layers, their aromatic fragments are perpendicular, which significantly reduces the contribution of the C . . . C contacts (0.4% vs. 4.9% on average). In contrast, their parallel arrangement in the co-crystal of gallic acid with 4-cyanopyridine (LALVED [41]) that allows them to form parallel-displaced stacking interactions (Figure S9 of Supplementary Materials) increases the corresponding value up to 8.0%.

A switch from the single-point acid–pyridine heterosynthon in these co-crystals to its two-point variant in **1**–**3** causes a weakening of the O-H . . . N/N-H . . . O hydrogen bond (Tables S2 and S4 of Supplementary Materials) by the competitive hydrogen bond with an *ortho*-substituent in the pyridine fragment. A proton-accepting group (C=O or COO^-) appearing in this position of the pyridine-containing compound adopting a tautomeric (**1** and **2**) or a zwitterionic form (**3**) triggers an increase (decrease) in the contribution of the O . . . H (N . . . H) contacts (Table 2 and Table S1 of Supplementary Materials).

In the crystals of the salts **4** and **5** with the two- to four-point heterosynthons, the contribution of the O . . . H contacts of the gallate anion (Table 3) featured as bright red spots on its Hirshfeld surfaces (Figure 5) is even higher than in the obtained co-crystals **1**–**3** (47.0 vs. 43.0% on average); the same is also true for the H . . . H and C . . . H contacts (27.4 vs. 24.7% and 17.2 vs. 12.0% on average). The formation of the four-point and two-point heterosynthons by two symmetry-independent gallate anions of the salt **4** causes differences in their crystal environment, such as higher contributions of H . . . O contacts (46.7 and 44.6%) or C . . . C contacts (4.9 and 3.3%) resulting from parallel-displaced stacking interactions formed by the four-point heterosynthon. In the salt **5**, the more efficient (as judged by geometric parameters) stacking interactions, which appear as flat white areas on the Hirshfeld surface and as the bright green cluster in the center of the corresponding 2D fingerprint plot, have a significantly larger contribution of 8.4% that makes it only second to the co-crystal **3** (12.4%) with an extended aromatic zwitterion of quinoline-2-carboxylic acid. The contribution of other types of interactions formed by the gallate anion in the salts **4** and **5** (Table 2) is below 3.1%.

Mirroring the co-crystals **1**–**3**, the salts **4** and **5** feature the multi-point heterosynthons (Scheme 1, center and right) instead of the single-point heterosynthon (Scheme 1, left) found in all the (ordered) gallate salts of pyridine-containing compounds [60,63–65,86] available in the Cambridge Structural Database (CCDC Version 2021.2.0) (Scheme 4), including the one of 3-hydroxypyridine (RefCode XUMKAU [63]). This difference, however, has only a minor effect on the contributions of interactions formed by the gallate anion (Figure S11 of Supplementary Materials). For the most important types of contacts in these salts (O . . . H, H . . . H, and C . . . H), the corresponding average values (47.7, 25.7, and 12.6%, respectively) are the same as in **4** and **5** within 1% (Table 3 and Table S5 of Supplementary Materials). Some 'local' differences arise due to distinctive features of the pyridine-containing compounds, such as an extended aromatic system or an additional neutral pyridine fragment.

Table 3. Contributions (%) of various interactions into the Hirshfeld surface of the gallate anion in **4** and **5**.

Contacts	4 *	5	Average
O . . . H	46.7 (44.6)	49.6	47.0
N . . . H	0.7 (0.2)	0.5	0.5
C . . . H	14.9 (18.2)	10.0	17.2
H . . . H	28.6 (30.1)	24.6	27.4
C . . . C	4.9 (3.3)	8.4	5.4
O . . . O	1.5 (1.3)	2.6	2.0
C . . . N	1.5 (0.8)	1.6	1.3
C . . . O	0.7 (1.0)	2.5	1.4
N . . . O	0.6 (0.3)	0.2	0.4

* The values for the second symmetry-independent gallate anion are given in parentheses.

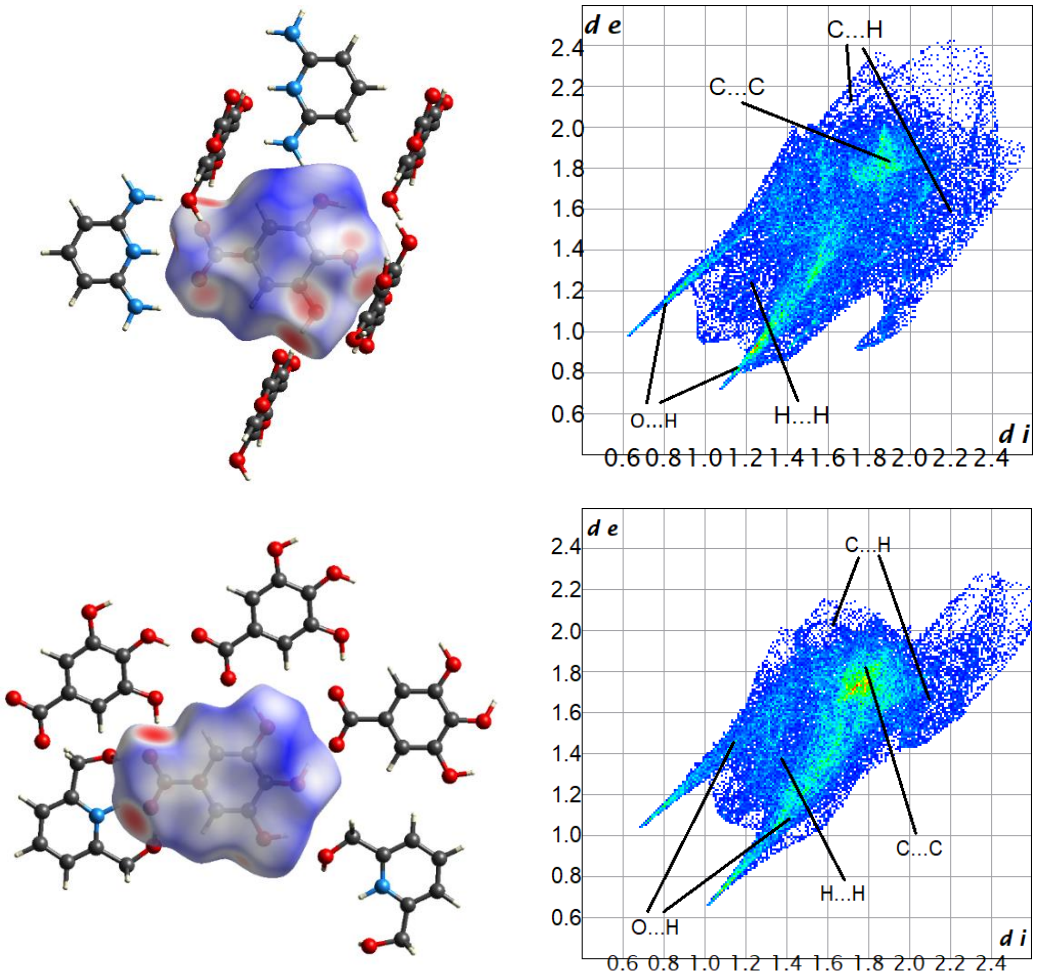

Figure 5. Hirshfeld surfaces (**left**) of the gallate anion in salts **4** (**top**) and **5** (**bottom**) and their 2D fingerprint plots (**right**) as generated by Crystal Explorer [83]. For the second symmetry-independent gallate anion in **4**, see Figure S10 of Supplementary Materials.

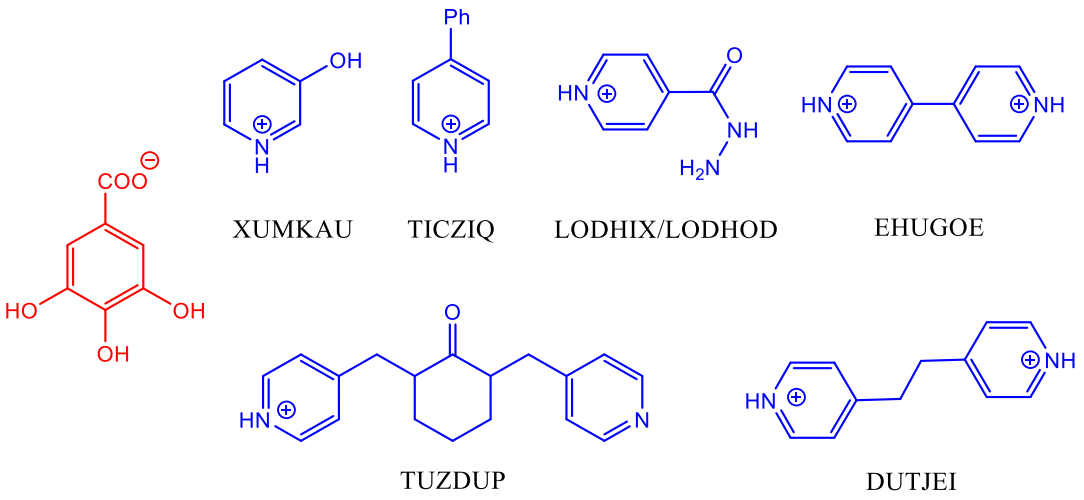

Scheme 4. Salts of gallic acid and pyridine-containing compounds and their RefCodes [60,63–66,86]. X-ray diffraction data for LODHIX and LODHOD are collected from the same salt at 100 K and at room temperature, respectively; LODHIX, LODHOD, EHUGOE, and DUTJEI also contain lattice water molecules.

In the salt of 4-phenylpyridine (TICZIQ [86]), the gallate anions are assembled into corrugated layers by hydrogen bonds between their carboxylate and hydroxyl groups (Figure S12 of Supplementary Materials), with a resulting increase in the contribution of O ... H contacts by 7% from an average value of 47.7% (Table S5 of Supplementary Materials). As their aromatic fragments are not involved in stacking interactions within or between these layers, the C ... C contacts have a zero contribution into the Hirshfeld surface of the gallate anion as compared to other salts (Table S5 of Supplementary Materials). In TUZDUP [60], the presence of a neutral pyridine fragment in addition to its protonated analogue in the appropriate cation is, apparently, behind the highest contribution of the N ... H contacts (3.1%) among the gallate salts adopting an average value of 0.8%.

Comparison of these salts and the above co-crystals of gallic acid reveals a larger contribution of the O ... H contacts in the former (47.7 vs. 39.3% on average) and of the N ... H contacts in the latter (0.8 vs. 7.3% on average), which nicely agrees with the location of the hydrogen atom in the heterosynthon on the pyridine species or on the acid molecule. The charge-assisted [87,88] N-H ... O hydrogen bond between the ions and O-H ... N hydrogen bond between the molecules, as judged by their geometric parameters (Tables S2 and S3 of Supplementary Materials), might explain [89,90] the occurrence of the acid–pyridine heterosynthon in all the salts but only in half of the co-crystals found in Cambridge Structural Database. A large difference in the above contributions in the co-crystal TUZFEB and the salt TUZDUP (30.7 vs. 44.2% and 9.8 vs. 3.1%) of structurally similar pyridine-containing compounds additionally arises from the hydrogen bonds between the gallate anions that are lacking in the former (Figure S13 of Supplementary Materials), and from the NMe moiety that is lacking in the later to produce O-H ... N hydrogen bonds with the molecules of gallic acid (Figure S7 of Supplementary Materials). A resulting coplanar arrangement of the two components in TUZDUP in contrast to their perpendicular arrangement in TUZFEB causes a significant increase in the contribution of the C ... C contacts (6.2 vs. 0.8%, respectively).

The co-crystals and salts of gallic acid and the above pyridine-containing compounds feature the common acid–pyridine heterosynthon, either neutral or ionic [47,50,51] (if any; Tables S2 and S3 of Supplementary Materials), modified by the *ortho*-substituents in **1**–**5** to adopt its various multi-point variants. While one such substituent can form another hydrogen bond with the carboxylic group to produce a two-point heterosynthon, the competition between the two identical proton-donating groups allows for the formation of the two- to four-point heterosynthons, with a proportional weakening of the O-H ... N/N-H ... O hydrogen bond (Tables S2 and S3 of Supplementary Materials). These additional hydrogen bonds, however, make the acid–pyridine heterosynthon preferred over the competing acid–acid homosynthon [48], which is found in almost half of the co-crystals of gallic acid and pyridine-containing compounds with no *ortho*-substituents. In the salts, the acid–acid homosynthon does not appear, owing to the carboxylate group lacking the proton-donating ability.

Depending on the choice of the pyridine-containing compound, the neutral or ionic nature of the resulting two-component system of gallic acid mostly follows the pKa rule [55,91–94] stating that a salt is formed if ΔpKa > 3 and a co-crystal, if ΔpKa < −1 (Table S6 of Supplementary Materials). The exceptions are the salt of 4,4′-ethylenedipyridin (DUTJEI), which is obtained with lattice water molecules [65] to affect the pKa values of the components [95], and of isoniazid (LODHIX and LODHOD), which is a superposition of a salt and a co-crystal not attained at the highest accessed temperature [64], as well as the previously reported co-crystal **1** [63] and its new solvatomorph **2**. In these co-crystals, the appropriate hydroxylpyridine adopts its keto-form (Scheme S1 of Supplementary Materials) preferred in the crystal state [67,68], thereby precluding the proton transfer to the nitrogen atom and the formation of a predicted salt. In the case of the salt **4** and a few reported co-crystals (XUMHUL, YAHTUY, AYIWEM, TUZFAX, and TUZFEB) and salts (TICZIQ, TUZDUP, and EHUGOE), the ΔpKa value for the two components is between −1 and 3 (Table S6 of Supplementary Materials), which is the gray zone for the prediction of

the proton transfer [55,64,86,92–94,96], so the formation of the salt and of the co-crystal is equally plausible.

4. Conclusions

Co-crystallization of gallic acid with *ortho*-substituted pyridines (2-hydroxypyridine, 2,6-diaminopyridine, 2,6-dimethylhydroxypyridine) and their polyaromatic analogue, quinoline-2-carboxylic acid, produced five crystalline products, including a previously reported co-crystal **1** with pyridone-2 [63]. The latter was, to the best of our knowledge, the only known product of gallic acid and an *ortho*-functionalized pyridine. The formation of the co-crystals or the salts depending on the choice of the pyridine-containing compound follows the pKa rule, the exceptions being the co-crystals **1** and **2**, owing to the preference of 2-hydroxypyridine to exist in the crystal state as pyridone-2 [67,68].

While most of the other two-component systems of gallic acid feature the popular single-point heterosynthon (Scheme 1, left), the use of a pyridine compound with one or two *ortho*-substituents that are able to form competitive hydrogen bonds successfully modifies this heterosynthon to produce its various multi-point variants (Scheme 1, center and right). Of them, the two- and three-point heterosynthons are often obtained for carboxylic acids, and the salt **4** of 2,6-diaminopyridine is the rare example of a four-point heterosynthon, which resulted from the competition of two identical proton-donating substituents for the formation of hydrogen bonds with the carboxylate group. A methylene bridge between these groups and the pyridine fragment in 2,6-dimethylhydroxypyridine prevents the two components from being in the same plane, thereby leading to their vertical shift in a more common three-point heterosynthon [78].

In a multi-point heterosynthon, the O-H . . . N/N-H . . . O hydrogen bond between the two components is weakened as compared to the single-point heterosynthon (judging by the interatomic distances O . . . N and the deviation of the angle NHO from the linearity) by the competing hydrogen bonds with the *ortho*-substituents of the pyridine fragment, as in similar systems of carboxylic acids and amino-substituted pyrimidines and imidazoles [90,97,98]. Such substituents, however, strongly favor the formation of the acid–pyridine heterosynthon over the acid–acid homosynthon also typical of carboxylic acids [84,99]. This might be used to reduce the supramolecular-synthon-based polymorphism [99,100] of a pharmaceutical [101–104] or to modify its physicochemical properties, such as to increase the solubility [105] and the dissolution rate of the pyridine-containing drug compound in an appropriate co-crystal/salt to improve its bioavailability [106,107]. On the other hand, the contributions of the intermolecular interactions formed by the molecule of gallic acid or the gallate anion that feature the single-point acid–pyridine heterosynthon are only slightly affected by the *ortho*-substituents in the pyridine-containing compound. Differences arise from its other structural features, such as the presence of an extended aromatic system, another neutral pyridine fragment, its preference to exist as a zwitterion or another tautomer, or from the presence of lattice solvents.

Co-crystallization of gallic acid with pyridines or their heterocyclic analogues *ortho*-substituted by functional groups able to form hydrogen bonds allows exploration of preferential occurrences of supramolecular synthons in the competitive conditions of such two-component systems and guiding of them towards the formation of various multi-point acid–pyridine heterosynthons—including those rarely observed before—to produce new pharmaceutical [17] and other crystalline materials with the designed properties.

Supplementary Materials: The following supporting information can be downloaded at: https://www.mdpi.com/article/10.3390/cryst12040497/s1, Figure S1: General view of the second symmetry-independent formula unit of the salt **4**. Hereinafter, non-hydrogen atoms are shown as thermal ellipsoids (p = 50%) and dashed lines stand for hydrogen bonds; Figure S2: Fragments of the crystal packing in the salt **4** that are produced by the two-point (top) and the four-point (bottom) acid–pyridine heterosynthons; Figure S3: A fragment of the crystal packing in the co-crystal XUMHUL illustrating the formation of a centrosymmetric homosynthon from the molecules of gallic acid; Figure S4: Fragments of the crystal packing in the co-crystals RUWGUM (top) and RUWHAT (bot-

tom), illustrating the formation of hydrogen-bonded chains from the zwitterions of isonicotinic or nicotinic acid; Figure S5: A fragment of the crystal packing in the salt AYIWEM, illustrating the formation of hydrogen-bonded dimers from the molecules of gallic acid; Figure S6: Hirshfeld surfaces (left) of the molecule of gallic acid and their 2D fingerprint plots (right), as generated by Crystal Explorer [1], in other co-crystals of gallic acid and pyridine-containing compounds from CSD identified by their RefCodes; Figure S7: Fragments of the crystal packing in the co-crystals TUZFAX (top) and TUZFEB (bottom), illustrating the formation of hydrogen-bonded layers from the molecules of gallic acid and of an appropriate pyridine-containing compound; Figure S8: A fragment of the crystal packing in the co-crystal LEFPUJ, illustrating the formation of hydrogen-bonded layers with alternating chains of the molecules of gallic acid and of 1,2-bis(pyridin-4-yl)diazene; Figure S9: A fragment of the crystal packing in the co-crystal LALVED, illustrating the formation of hydrogen-bonded chains from the molecules of gallic acid and 4-cyanopyridine; Figure S10: Hirshfeld surface (left) of the second symmetry-independent gallate anion in the salt **4** and its 2D fingerprint plot (right); Figure S11: Hirshfeld surfaces (left) of the gallate anion and their 2D fingerprint plots (right) in other salts of gallic acid and pyridine-containing compounds from CSD identified by their RefCodes. X-ray diffraction data for LODHIX and LODHOD are collected from the same salt at 100 K and at room temperature, respectively; Figure S12: A fragment of the crystal packing in the salt TICZIQ, illustrating the formation of hydrogen-bonded corrugated layers from the gallate anions; Figure S13: A fragment of the crystal packing in the co-crystal TUZDUP, illustrating the formation of hydrogen-bonded layers; Scheme S1: Keto–enol equilibrium of 2-OH-Py favoring its keto-form, pyridone-2; Table S1: Contributions (%) of various interactions into the Hirshfeld surface of the molecule of gallic acid in other co-crystals of gallic acid identified by their RefCodes in CSD; Table S2: The parameters of the hydrogen bond O-H . . . N in the heterosynthon acid–pyridine in the co-crystals of gallic acid identified by their RefCodes in CSD; Table S3: The parameters of the hydrogen bond N-H . . . O in the heterosynthon acid–pyridine in the gallate salts identified by their RefCodes in CSD; Table S4: The parameters of the hydrogen bond N-H . . . O in the heterosynthon acid–pyridine in the co-crystals **1**, **2**, and **3** and in the salts **4** and **5** together with the appropriate average values; Table S5: Contributions (%) of various interactions into the Hirshfeld surface of the gallate anion in other gallate salts identified by their RefCodes in CSD; Table S6: ΔpKa values for **1**–**5** and for other two-component systems based on gallic acid identified by their RefCodes in CSD.

Author Contributions: Conceptualization, Y.V.N.; methodology, G.L.D.; software, G.L.D.; validation, G.L.D. and Y.V.N.; formal analysis, G.L.D.; investigation, G.L.D.; resources, Y.V.N.; data curation, Y.V.N.; writing—original draft preparation, G.L.D. and Y.V.N.; writing—review and editing, Y.V.N.; visualization, G.L.D.; supervision, Y.V.N.; project administration, Y.V.N.; funding acquisition, Y.V.N. All authors have read and agreed to the published version of the manuscript.

Funding: This research was supported by the Russian Science Foundation (Project 20-73-10200). Elemental analysis was performed with the financial support from the Ministry of Science and Higher Education of the Russian Federation using the equipment of the Center for molecular composition studies of INEOS RAS.

Institutional Review Board Statement: Not applicable.

Informed Consent Statement: Not applicable.

Data Availability Statement: Not applicable.

Conflicts of Interest: The authors declare no conflict of interest.

References

1. Desiraju, G.R. Crystal Engineering: A Holistic View. *Angew. Chem. Int. Ed.* **2007**, *46*, 8342–8356. [CrossRef] [PubMed]
2. Whitesides, G.M.; Simanek, E.E.; Mathias, J.P.; Seto, C.T.; Chin, D.; Mammen, M.; Gordon, D.M. Noncovalent Synthesis: Using Physical-Organic Chemistry to Make Aggregates. *Acc. Chem. Res.* **1995**, *28*, 37–44. [CrossRef]
3. Steiner, T. The Hydrogen Bond in the Solid State. *Angew. Chem. Int. Ed.* **2002**, *41*, 48–76. [CrossRef]
4. Nishio, M. CH/π Hydrogen Bonds in Crystals. *CrystEngComm* **2004**, *6*, 130–158. [CrossRef]
5. Ma, J.C.; Dougherty, D.A. The Cation−π Interaction. *Chem. Rev.* **1997**, *97*, 1303–1324. [CrossRef] [PubMed]
6. Claessens, C.G.; Stoddart, J.F. π–π Interactions in Self-Assembly. *J. Phys. Org. Chem.* **1997**, *10*, 254–272. [CrossRef]
7. Desiraju, G.R. Supramolecular Synthons in Crystal Engineering—A New Organic Synthesis. *Angew. Chem. Int. Ed. Engl.* **1995**, *34*, 2311–2327. [CrossRef]

8. Krishnamohan, S.; Zaworotko, M.J. X-Ray Crystal Structure of C6H3(CO2H)3-1,3,5·1.5(4,4′-Bipy): A 'Super Trimesic Acid' Chicken-Wire Grid. *Chem. Commun.* **1996**, *23*, 2655–2656. [CrossRef]
9. Dale, S.H.; Elsegood, M.R.J.; Hemmings, M.; Wilkinson, A.L. The Co-Crystallisation of Pyridine with Benzenepolycarboxylic Acids: The Interplay of Strong and Weak Hydrogen Bonding Motifs. *CrystEngComm* **2004**, *6*, 207–214. [CrossRef]
10. Vishweshwar, P.; Nangia, A.; Lynch, V.M. Recurrence of Carboxylic Acid−Pyridine Supramolecular Synthon in the Crystal Structures of Some Pyrazinecarboxylic Acids. *J. Org. Chem.* **2002**, *67*, 556–565. [CrossRef] [PubMed]
11. Aakeröy, C.B.; Beatty, A.M.; Helfrich, B.A. "Total Synthesis" Supramolecular Style: Design and Hydrogen-Bond-Directed Assembly of Ternary Supermolecules. *Angew. Chem. Int. Ed.* **2001**, *40*, 3240–3242. [CrossRef]
12. Eddaoudi, M.; Moler, D.B.; Li, H.; Chen, B.; Reineke, T.M.; O'Keeffe, M.; Yaghi, O.M. Modular Chemistry: Secondary Building Units as a Basis for the Design of Highly Porous and Robust Metal−Organic Carboxylate Frameworks. *Acc. Chem. Res.* **2001**, *34*, 319–330. [CrossRef] [PubMed]
13. Moulton, B.; Zaworotko, M.J. From Molecules to Crystal Engineering: Supramolecular Isomerism and Polymorphism in Network Solids. *Chem. Rev.* **2001**, *101*, 1629–1658. [CrossRef] [PubMed]
14. Braga, D.; Maini, L.; Polito, M.; Scaccianoce, L.; Cojazzi, G.; Grepioni, F. Design of Organometallic Molecular and Ionic Materials. *Coord. Chem. Rev.* **2001**, *216–217*, 225–248. [CrossRef]
15. Thallapally, P.K.; Wirsig, T.B.; Barbour, L.J.; Atwood, J.L. Crystal Engineering of Nonporous Organic Solids for Methane Sorption. *Chem. Commun.* **2005**, *35*, 4420–4422. [CrossRef] [PubMed]
16. Mohanta, S.; Lin, H.H.; Lee, C.J.; Wei, H.H. A Two-Dimensional CuIIGdIII Compound Self-Assembled by H-Bonding and Intermolecular Weak Coordinate Bonding between the Dinuclear Cores: Structure and Magnetic Properties. *Inorg. Chem. Commun.* **2002**, *5*, 585–588. [CrossRef]
17. Berry, D.J.; Steed, J.W. Pharmaceutical Cocrystals, Salts and Multicomponent Systems; Intermolecular Interactions and Property Based Design. *Adv. Drug Deliv. Rev.* **2017**, *117*, 3–24. [CrossRef] [PubMed]
18. Almarsson, Ö.; Zaworotko, M.J. Crystal Engineering of the Composition of Pharmaceutical Phases. Do Pharmaceutical Co-Crystals Represent a New Path to Improved Medicines? *Chem. Commun.* **2004**, *17*, 1889–1896. [CrossRef]
19. Etter, M.C. Hydrogen Bonds as Design Elements in Organic Chemistry. Available online: https://pubs.acs.org/doi/pdf/10.1021/j100165a007 (accessed on 11 February 2021).
20. Shattock, T.R.; Arora, K.K.; Vishweshwar, P.; Zaworotko, M.J. Hierarchy of Supramolecular Synthons: Persistent Carboxylic Acid·Pyridine Hydrogen Bonds in Cocrystals That also Contain a Hydroxyl Moiety. *Cryst. Growth Des.* **2008**, *8*, 4533–4545. [CrossRef]
21. Chitra, R.; Choudhury, R.R.; Thiruvenkatam, V.; Hosur, M.V.; Guru Row, T.N. Molecular Interactions in Bis(2-Aminopyridinium) Malonate: A Crystal Isostructural to Bis(2-Aminopyridinium) Maleate Crystal. *J. Mol. Struct.* **2012**, *1010*, 46–51. [CrossRef]
22. Varughese, S.; Pedireddi, V.R. A Competitive Molecular Recognition Study: Syntheses and Analysis of Supramolecular Assemblies of 3,5-Dihydroxybenzoic Acid and Its Bromo Derivative with Some N-Donor Compounds. *Chem.-A Eur. J.* **2006**, *12*, 1597–1609. [CrossRef]
23. Gunawardana, C.A.; Aakeröy, C.B. Co-Crystal Synthesis: Fact, Fancy, and Great Expectations. *Chem. Commun.* **2018**, *54*, 14047–14060. [CrossRef]
24. Ponce, A.; Brostoff, L.B.; Gibbons, S.K.; Zavalij, P.; Viragh, C.; Hooper, J.; Alnemrat, S.; Gaskell, K.J.; Eichhorn, B. Elucidation of the Fe(III) Gallate Structure in Historical Iron Gall Ink. *Anal. Chem.* **2016**, *88*, 5152–5158. [CrossRef]
25. Dewick, P.M.; Haslam, E. Phenol Biosynthesis in Higher Plants. Gallic Acid. *Biochem. J.* **1969**, *113*, 537–542. [CrossRef] [PubMed]
26. Ow, Y.Y.; Stupans, I. Gallic Acid and Gallic Acid Derivatives: Effects on Drug Metabolizing Enzymes. *Curr. Drug Metab.* **2003**, *4*, 241–248. [CrossRef] [PubMed]
27. Souza, L.P.; Calegari, F.; Zarbin, A.J.; Marcolino-Junior, L.H.; Bergamini, M.F. Voltammetric Determination of the Antioxidant Capacity in Wine Samples Using a Carbon Nanotube Modified Electrode. *J. Agric. Food Chem.* **2011**, *59*, 7620–7625. [CrossRef] [PubMed]
28. Özçelik, B.; Kartal, M.; Orhan, I. Cytotoxicity, Antiviral and Antimicrobial Activities of Alkaloids, Flavonoids, and Phenolic Acids. *Pharm. Biol.* **2011**, *49*, 396–402. [CrossRef] [PubMed]
29. Liu, K.C.; Huang, A.C.; Wu, P.P.; Lin, H.Y.; Chueh, F.S.; Yang, J.S.; Lu, C.C.; Chiang, J.H.; Meng, M.; Chung, J.G. Gallic Acid Suppresses the Migration and Invasion of PC-3 Human Prostate Cancer Cells via Inhibition of Matrix Metalloproteinase-2 and -9 Signaling Pathways. *Oncol. Rep.* **2011**, *26*, 177–184. [CrossRef] [PubMed]
30. Lu, Y.; Jiang, F.; Jiang, H.; Wu, K.; Zheng, X.; Cai, Y.; Katakowski, M.; Chopp, M.; To, S.S.T. Gallic Acid Suppresses Cell Viability, Proliferation, Invasion and Angiogenesis in Human Glioma Cells. *Eur. J. Pharmacol.* **2010**, *641*, 102–107. [CrossRef] [PubMed]
31. Priscilla, D.H.; Prince, P.S.M. Cardioprotective Effect of Gallic Acid on Cardiac Troponin-T, Cardiac Marker Enzymes, Lipid Peroxidation Products and Antioxidants in Experimentally Induced Myocardial Infarction in Wistar Rats. *Chem.-Biol. Interact.* **2009**, *179*, 118–124. [CrossRef]
32. Clarke, H.D.; Arora, K.K.; Wojtas, Ł.; Zaworotko, M.J. Polymorphism in Multiple Component Crystals: Forms III and IV of Gallic Acid Monohydrate. *Cryst. Growth Des.* **2011**, *11*, 964–966. [CrossRef]
33. Zhao, X.; Zhang, W.; Kong, S.; Zheng, X.; Zheng, J.; Shi, R. A Valid Assay for the Pharmacokinetic Study of Gallic Acid from Choerospondiatis Fructus in Rabbit Plasma by LC/MS/MS. *J. Liq. Chromatogr. Relat. Technol.* **2007**, *30*, 235–244. [CrossRef]

34. Jo, C.R.; Jeong, I.Y.; Lee, N.Y.; Kim, K.S.; Byun, M.W. Synthesis of a Novel Compound from Gallic Acid and Linoleic Acid and Its Biological Functions. *Food Sci. Biotechnol.* **2006**, *15*, 317–320.
35. Maldonado, O.S.; Lucas, R.; Comelles, F.; González, M.J.; Parra, J.L.; Medina, I.; Morales, J.C. Synthesis and Characterization of Phenolic Antioxidants with Surfactant Properties: Glucosyl-and Glucuronosyl Alkyl Gallates. *Tetrahedron* **2011**, *67*, 7268–7279. [CrossRef]
36. Braun, D.E.; Bhardwaj, R.M.; Florence, A.J.; Tocher, D.A.; Price, S.L. Complex Polymorphic System of Gallic Acid—Five Monohydrates, Three Anhydrates, and over 20 Solvates. *Cryst. Growth Des.* **2013**, *13*, 19–23. [CrossRef] [PubMed]
37. Song, J.X.; Chen, J.M.; Lu, T.B. Lenalidomide–Gallic Acid Cocrystals with Constant High Solubility. *Cryst. Growth Des.* **2015**, *15*, 4869–4875. [CrossRef]
38. Surov, A.O.; Churakov, A.V.; Proshin, A.N.; Dai, X.L.; Lu, T.; Perlovich, G.L. Cocrystals of a 1,2,4-Thiadiazole-Based Potent Neuroprotector with Gallic Acid: Solubility, Thermodynamic Stability Relationships and Formation Pathways. *Phys. Chem. Chem. Phys.* **2018**, *20*, 14469–14481. [CrossRef] [PubMed]
39. Pantwalawalkar, J.; More, H.; Bhange, D.; Patil, U.; Jadhav, N. Novel Curcumin Ascorbic Acid Cocrystal for Improved Solubility. *J. Drug Deliv. Sci. Technol.* **2021**, *61*, 102233. [CrossRef]
40. Gandhi, A.K.; Shi, T.; Li, M.; Jungnelius, U.; Romano, A.; Tabernero, J.; Siena, S.; Schafer, P.H.; Chopra, R. Immunomodulatory Effects in a Phase II Study of Lenalidomide Combined with Cetuximab in Refractory KRAS-Mutant Metastatic Colorectal Cancer Patients. *PLoS ONE* **2013**, *8*, e80437. [CrossRef]
41. Goswami, S.; Ghosh, A.; Borah, K.; Mahanta, A.; Guha, A.K.; Bora, S.J. Structure-Property Correlation in Gallic Acid and 4-Cyanopyridine Cocrystal and Binding Studies with Drug Efflux Pump in Bacteria. *J. Mol. Struct.* **2021**, *1225*, 129279. [CrossRef]
42. Chen, J.M.; Li, S.; Lu, T.B. Pharmaceutical Cocrystals of Ribavirin with Reduced Release Rates. *Cryst. Growth Des.* **2014**, *14*, 6399–6408. [CrossRef]
43. Wang, Z.; Gu, H.; Chen, W. Synthesis, Characterization and Antimicrobial Activity of Three Gallates Containing Imidazole, Benzimidazole and Triclosan Units. *Asian J. Chem.* **2014**, *26*, 513–520. [CrossRef]
44. Steiner, T. Competition of Hydrogen-Bond Acceptors for the Strong Carboxyl Donor. *Acta Crystallogr. Sect. B Struct. Sci.* **2001**, *57*, 103–106. [CrossRef] [PubMed]
45. McMahon, J.A.; Bis, J.A.; Vishweshwar, P.; Shattock, T.R.; McLaughlin, O.L.; Zaworotko, M.J. Crystal Engineering of the Composition of Pharmaceutical Phases. 3. Primary Amide Supramolecular Heterosynthons and Their Role in the Design of Pharmaceutical Co-Crystals. *Z. Für Krist.-Cryst. Mater.* **2005**, *220*, 340–350. [CrossRef]
46. Bora, P.; Saikia, B.; Sarma, B. Regulation of Π···π Stacking Interactions in Small Molecule Cocrystals and/or Salts for Physiochemical Property Modulation. *Cryst. Growth Des.* **2018**, *18*, 1448–1458. [CrossRef]
47. Sarma, B.; Nath, N.K.; Bhogala, B.R.; Nangia, A. Synthon Competition and Cooperation in Molecular Salts of Hydroxybenzoic Acids and Aminopyridines. *Cryst. Growth Des.* **2009**, *9*, 1546–1557. [CrossRef]
48. Hemamalini, M.; Loh, W.S.; Quah, C.K.; Fun, H.K. Investigation of Supramolecular Synthons and Structural Characterisation of Aminopyridine-Carboxylic Acid Derivatives. *Chem. Cent. J.* **2014**, *8*, 31. [CrossRef] [PubMed]
49. Lemmerer, A.; Govindraju, S.; Johnston, M.; Motloung, X.; Savig, K.L. Co-Crystals and Molecular Salts of Carboxylic Acid/Pyridine Complexes: Can Calculated p K a's Predict Proton Transfer? A Case Study of Nine Complexes. *CrystEngComm* **2015**, *17*, 3591–3595. [CrossRef]
50. Allen, F.H.; Motherwell, W.D.S.; Raithby, P.R.; Shields, G.P.; Taylor, R. Systematic Analysis of the Probabilities of Formation of Bimolecular Hydrogen-Bonded Ring Motifs in Organic Crystal Structures. *New J. Chem.* **1999**, *23*, 25–34. [CrossRef]
51. Mohamed, S.; Tocher, D.A.; Vickers, M.; Karamertzanis, P.G.; Price, S.L. Salt or Cocrystal? A New Series of Crystal Structures Formed from Simple Pyridines and Carboxylic Acids. *Cryst. Growth Des.* **2009**, *9*, 288–2889. [CrossRef]
52. Mukherjee, A.; Desiraju, G.R. Combinatorial Exploration of the Structural Landscape of Acid–Pyridine Cocrystals. *Cryst. Growth Des.* **2014**, *14*, 1375–1385. [CrossRef]
53. Aakeröy, C.B.; Fasulo, M.E.; Desper, J. Cocrystal or Salt: Does It Really Matter? *Mol. Pharm.* **2007**, *4*, 317–322. [CrossRef]
54. Aitipamula, S.; Banerjee, R.; Bansal, A.K.; Biradha, K.; Cheney, M.L.; Choudhury, A.R.; Desiraju, G.R.; Dikundwar, A.G.; Dubey, R.; Duggirala, N.; et al. Polymorphs, Salts, and Cocrystals: What's in a Name? *Cryst. Growth Des.* **2012**, *12*, 2147–2152. [CrossRef]
55. Childs, S.L.; Stahly, G.P.; Park, A. The Salt−Cocrystal Continuum: The Influence of Crystal Structure on Ionization State. *Mol. Pharm.* **2007**, *4*, 323–338. [CrossRef] [PubMed]
56. Gutmann, F. *Charge Transfer Complexes in Biological Systems*; M. Dekker: New York, NY, USA, 1997; ISBN 0-8247-9986-0.
57. Khan, I.M.; Ahmad, A. Synthesis, Characterization, Structural, Spectrophotometric and Antimicrobial Activity of Charge Transfer Complex of p-Phenylenediamine with 3,5-Dinitrosalicylic Acid. *J. Mol. Struct.* **2010**, *975*, 381–388. [CrossRef]
58. Khan, I.M.; Ahmad, A.; Aatif, M. Synthesis, Single-Crystal Characterization, Antimicrobial Activity and Remarkable In Vitro DNA Interaction of Hydrogen-Bonded Proton-Transfer Complex of 1,10-Phenanthroline with 2,4,6-Trinitrophenol. *J. Photochem. Photobiol. B Biol.* **2011**, *105*, 6–13. [CrossRef] [PubMed]
59. Aitipamula, S.; Chow, P.S.; Tan, R.B. Polymorphism in Cocrystals: A Review and Assessment of Its Significance. *CrystEngComm* **2014**, *16*, 3451–3465. [CrossRef]
60. Liu, L.D.; Liu, S.L.; Liu, Z.X.; Hou, G.G. Synthesis, Structure, Antitumor Activity of Novel Pharmaceutical Co-Crystals Based on Bispyridyl-Substituted α, β-Unsaturated Ketones with Gallic Acid. *J. Mol. Struct.* **2016**, *1112*, 1–8. [CrossRef]

61. Kavuru, P.; Aboarayes, D.; Arora, K.K.; Clarke, H.D.; Kennedy, A.; Marshall, L.; Ong, T.T.; Perman, J.; Pujari, T.; Wojtas, Ł.; et al. Hierarchy of Supramolecular Synthons: Persistent Hydrogen Bonds between Carboxylates and Weakly Acidic Hydroxyl Moieties in Cocrystals of Zwitterions. *Cryst. Growth Des.* **2010**, *10*, 3568–3584. [CrossRef]
62. Dong, F.Y.; Wu, J.; Tian, H.Y.; Ye, Q.M.; Jiang, R.W. Gallic Acid Pyridine Monosolvate. *Acta Crystallogr. Sect. E Struct. Rep. Online* **2011**, *67*, o3096. [CrossRef] [PubMed]
63. Jyothi, K.L.; Kumara, K.; Hema, M.K.; Mahesha; Gautam, R.; Guru Row, T.N.; Lokanath, N.K. Structural Elucidation, Theoretical Insights and Thermal Properties of Three Novel Multicomponent Molecular Forms of Gallic Acid with Hydroxypyridines. *J. Mol. Struct.* **2020**, *1207*, 127828. [CrossRef]
64. Kaur, R.; Perumal, S.S.R.R.; Bhattacharyya, A.J.; Yashonath, S.; Guru Row, T.N. Structural Insights into Proton Conduction in Gallic Acid—Isoniazid Cocrystals. *Cryst. Growth Des.* **2014**, *14*, 423–426. [CrossRef]
65. Shen, F.M.; Lush, S.F. 4,4′-Ethyl enedipyridinium Bis (3,4,5-Trihy droxy benzoate) Sesquihydrate. *Acta Crystallogr. Sect. E Struct. Rep. Online* **2010**, *66*, o2056–o2057. [CrossRef] [PubMed]
66. Zhao, X.; Wang, Q.; Qing, X.; Yu, H.; Wang, G. Crystal structure of 4,4′-bipyridine—3,4,5-trihydroxybenzoic acid—water (1:2:2), C10H8N2·2C7H6O5·2H2O. *Z. Für Krist.-New Cryst. Struct.* **2010**, *225*, 701–702. [CrossRef]
67. De Kowalewski, D.G.; Contreras, R.H.; Díez, E.; Esteban, A. NMR J(C,C) Scalar Coupling Analysis of the Effects of Substituents on the Keto–Enol Tautomeric Equilibrium in 2-OH-n-X-Pyridines. An Experimental and DFT Study. *Mol. Phys.* **2004**, *102*, 2607–2615. [CrossRef]
68. Yang, H.W.; Craven, B.M. Charge Density Study of 2-Pyridone. *Acta Crystallogr. Sect. B Struct. Sci.* **1998**, *54*, 912–920. [CrossRef]
69. Zhoujin, Y.; Yang, X.; Zhang, M.; Guo, J.; Parkin, S.; Li, T.; Yu, F.; Long, S. Synthon Polymorphism and π–π Stacking in N-Phenyl-2-Hydroxynicotinanilides. *Cryst. Growth Des.* **2021**, *21*, 6155–6165. [CrossRef]
70. Li, P.; Zhao, C.; Smith, M.D.; Shimizu, K.D. Comprehensive Experimental Study of N-Heterocyclic π-Stacking Interactions of Neutral and Cationic Pyridines. *J. Org. Chem.* **2013**, *78*, 5303–5313. [CrossRef]
71. Campos-Gaxiola, J.J.; García-Grajeda, B.A.; Hernández-Ahuactzi, I.F.; Guerrero-Álvarez, J.A.; Höpfl, H.; Cruz-Enríquez, A. Supramolecular Networks in Molecular Complexes of Pyridine Boronic Acids and Polycarboxylic Acids: Synthesis, Structural Characterization and Fluorescence Properties. *CrystEngComm* **2017**, *19*, 3760–3775. [CrossRef]
72. Dolomanov, O.V.; Bourhis, L.J.; Gildea, R.J.; Howard, J.A.; Puschmann, H. OLEX2: A Complete Structure Solution, Refinement and Analysis Program. *J. Appl. Cryst.* **2009**, *42*, 339–341. [CrossRef]
73. Sheldrick, G.M. SHELXT—Integrated Space-Group and Crystal-Structure Determination. *Acta Crystallogr. Sect. A Found. Adv.* **2015**, *71*, 3–8. [CrossRef]
74. Sheldrick, G.M. A Short History of SHELX. *Acta Crystallogr. Sect. A Found. Crystallogr. Acta* **2008**, *64*, 112–122. [CrossRef] [PubMed]
75. Hao, H.; Hou, B.; Wang, J.K.; Lin, G. Effect of Solvent on Crystallization Behavior of Xylitol. *J. Cryst. Growth* **2006**, *290*, 192–196. [CrossRef]
76. Nechipadappu, S.K.; Trivedi, D.R. Pharmaceutical Salts of Ethionamide with GRAS Counter Ion Donors to Enhance the Solubility. *Eur. J. Pharm. Sci.* **2017**, *96*, 578–589. [CrossRef]
77. Khan, I.M.; Ahmad, A.; Kumar, S. Synthesis, Spectroscopic Characterization and Structural Investigations of a New Charge Transfer Complex of 2,6-Diaminopyridine with 3,5-Dinitrobenzoic Acid: DNA Binding and Antimicrobial Studies. *J. Mol. Struct.* **2013**, *1035*, 38–45. [CrossRef]
78. Draguta, S.; Fonari, M.S.; Bejagam, S.N.; Storms, K.; Lindline, J.; Timofeeva, T.V. Structural Similarities and Diversity in a Series of Crystalline Solids Composed of 2-Aminopyridines and Glutaric Acid. *Struct. Chem.* **2016**, *27*, 1303–1315. [CrossRef]
79. Gao, X.; Zhang, H.; Wen, X.; Liu, B.; Jin, S.; Wang, D. Structure of Seven Organic Salts Assembled from 2,6-Diaminopyridine with Monocarboxylic Acids, Dicarboxylic Acids, and Tetracarboxylic Acids. *J. Mol. Struct.* **2015**, *1093*, 82–95. [CrossRef]
80. Blackholly, L.R.; Shepherd, H.J.; Hiscock, J.R. 'Frustrated' Hydrogen Bond Mediated Amphiphile Self-Assembly—A Solid State Study. *CrystEngComm* **2016**, *18*, 7021–7028. [CrossRef]
81. Spackman, M.A.; Jayatilaka, D. Hirshfeld Surface Analysis. *CrystEngComm* **2009**, *11*, 19–32. [CrossRef]
82. Spackman, M.A.; McKinnon, J.J. Fingerprinting Intermolecular Interactions in Molecular Crystals. *CrystEngComm* **2002**, *4*, 378–392. [CrossRef]
83. Spackman, P.R.; Turner, M.J.; McKinnon, J.J.; Wolff, S.K.; Grimwood, D.J.; Jayatilaka, D.; Spackman, M.A. CrystalExplorer: A Program for Hirshfeld Surface Analysis, Visualization and Quantitative Analysis of Molecular Crystals. *J. Appl. Cryst.* **2021**, *54*, 1006–1011. [CrossRef]
84. Long, S.; Li, T. Enforcing Molecule's π-Conjugation and Consequent Formation of the Acid−Acid Homosynthon over the Acid−Pyridine Heterosynthon in 2-Anilinonicotinic Acids. *Cryst. Growth Des.* **2010**, *10*, 2465–2469. [CrossRef]
85. Rusu, E.; Shova, S.; Rusu, G. 1,2-Bis(Pyridin-4-Yl)Diazene–3,4,5-Trihy droxy benzoic Acid–Methanol (3/2/2). *Acta Crystallogr. Sect. E Struct. Rep. Online* **2012**, *68*, o2436. [CrossRef] [PubMed]
86. Seaton, C.C.; Munshi, T.; Williams, S.E.; Scowen, I.J. Multi-Component Crystals of 4-Phenylpyridine: Challenging the Boundaries between Co-Crystal and Organic Salt Formation with Insight into Solid-State Proton Transfer. *CrystEngComm* **2013**, *15*, 5250–5260. [CrossRef]
87. Gilli, P.; Pretto, L.; Bertolasi, V.; Gilli, G. Predicting Hydrogen-Bond Strengths from Acid-Base Molecular Properties. The PK(a) Slide Rule: Toward the Solution of a Long-Lasting Problem. *Acc. Chem. Res.* **2009**, *42*, 33–44. [CrossRef] [PubMed]

88. Kochanek, S.E.; Clymer, T.M.; Pakkala, V.S.; Hebert, S.P.; Reeping, K.; Firestine, S.M.; Evanseck, J.D. Intramolecular Charge-Assisted Hydrogen Bond Strength in Pseudochair Carboxyphosphate. *J. Phys. Chem. B* **2015**, *119*, 1184–1191. [CrossRef]
89. Sedghiniya, S.; Soleimannejad, J.; Janczak, J. The Salt–Cocrystal Spectrum in Salicylic Acid–Adenine: The Influence of Crystal Structure on Proton-Transfer Balance. *Acta Crystallogr. Sect. C Struct. Chem.* **2019**, *75*, 412–421. [CrossRef]
90. Garg, U.; Azim, Y.; Kar, A.; Pradeep, C.P. Cocrystals/Salt of 1-Naphthaleneacetic Acid and Utilizing Hirshfeld Surface Calculations for Acid–Aminopyrimidine Synthons. *CrystEngComm* **2020**, *22*, 2978–2989. [CrossRef]
91. Huang, K.S.; Britton, D.; Byrn, S.R. A Novel Class of Phenol–Pyridine Co-Crystals for Second Harmonic Generation. *J. Mater. Chem.* **1997**, *7*, 713–720. [CrossRef]
92. Cruz-Cabeza, A.J. Acid–Base Crystalline Complexes and the pK_a Rule. *CrystEngComm* **2012**, *14*, 6362–6365. [CrossRef]
93. Bekö, S.L.; Schmidt, M.U.; Bond, A.D. An Experimental Screen for Quinoline /Fumaric Acid Salts and Co-Crystals. *CrystEngComm* **2012**, *14*, 1967–1971. [CrossRef]
94. Stilinović, V.; Kaitner, B. Salts and Co-Crystals of Gentisic Acid with Pyridine Derivatives: The Effect of Proton Transfer on the Crystal Packing (and Vice Versa). *Cryst. Growth Des.* **2012**, *12*, 5763–5772. [CrossRef]
95. Wróbel, R.; Chmurzyński, L. Potentiometric PKa Determination of Standard Substances in Binary Solvent Systems. *Anal. Chim. Acta* **2000**, *405*, 303–308. [CrossRef]
96. Delori, A.; Galek, P.T.; Pidcock, E.; Patni, M.; Jones, W. Knowledge-Based Hydrogen Bond Prediction and the Synthesis of Salts and Cocrystals of the Anti-Malarial Drug Pyrimethamine with Various Drug and GRAS Molecules. *CrystEngComm* **2013**, *15*, 2916–2928. [CrossRef]
97. Hu, Y.; Hu, H.; Li, Y.; Chen, R.; Yang, Y.; Wang, L. Supramolecular Assemblies of Tetrafluoroterephthalic Acid and N-Heterocycles via Various Strong Hydrogen Bonds and Weak CH$\cdots$F Interactions: Synthons Cooperation, Robust Motifs and Structural Diversity. *J. Mol. Struct.* **2016**, *1122*, 256–267. [CrossRef]
98. Pang, Y.; Xing, P.; Geng, X.; Zhu, Y.; Liu, F.; Wang, L. Supramolecular Assemblies of 2-Hydroxy-3-Naphthoic Acid and N-Heterocycles via Various Strong Hydrogen Bonds and Weak X$\cdots\pi$ (X = C–H, π) Interactions. *RSC Adv.* **2015**, *5*, 40912–40923. [CrossRef]
99. Basu, T.; Sparkes, H.A.; Mondal, R. Construction of Extended Molecular Networks with Heterosynthons in Cocrystals of Pyrazole and Acids. *Cryst. Growth Des.* **2009**, *9*, 5164–5175. [CrossRef]
100. Jetti, R.K.R.; Boese, R.; Sarma, J.A.R.P.; Reddy, L.S.; Vishweshwar, P.; Desiraju, G.R. Auf Der Suche Nach Einem Polymorph: Eine Zweite Kristallform von 6-Amino-2-Phenylsulfonylimino-1,2-Dihydropyridin. *Angew. Chem.* **2003**, *115*, 2008–2012. [CrossRef]
101. Sreekanth, B.R.; Vishweshwar, P.; Vyas, K. Supramolecular Synthon Polymorphism in 2:1 Co-Crystal of 4-Hydroxybenzoic Acid and 2,3,5,6-Tetramethylpyrazine. *Chem. Commun.* **2007**, *23*, 2375–2377. [CrossRef]
102. Kumar, S.S.; Nangia, A. A Solubility Comparison of Neutral and Zwitterionic Polymorphs. *Cryst. Growth Des.* **2014**, *14*, 1865–1881. [CrossRef]
103. Cao, H.L.; Zhou, J.R.; Cai, F.Y.; Lü, J.; Cao, R. Two-Component Pharmaceutical Cocrystals Regulated by Supramolecular Synthons Comprising Primary N$\cdots$H$\cdots$O Interactions. *Cryst. Growth Des.* **2019**, *19*, 3–16. [CrossRef]
104. Babu, N.J.; Cherukuvada, S.; Thakuria, R.; Nangia, A. Conformational and Synthon Polymorphism in Furosemide (Lasix). *Cryst. Growth Des.* **2010**, *10*, 1979–1989. [CrossRef]
105. Aitipamula, S.; Wong, A.B.; Chow, P.S.; Tan, R.B. Cocrystallization with Flufenamic Acid: Comparison of Physicochemical Properties of Two Pharmaceutical Cocrystals. *CrystEngComm* **2014**, *16*, 5793–5801. [CrossRef]
106. Wang, L.; Tan, B.; Zhang, H.; Deng, Z. Pharmaceutical Cocrystals of Diflunisal with Nicotinamide or Isonicotinamide. *Org. Process Res. Dev.* **2013**, *17*, 1413–1418. [CrossRef]
107. Bavishi, D.D.; Borkhataria, C.H. Spring and Parachute: How Cocrystals Enhance Solubility. *Prog. Cryst. Growth Charact. Mater.* **2016**, *62*, 1–8. [CrossRef]